International Journal of Heat and Mass Transfer 52 (2009) 5122–5129

Contents lists available at ScienceDirect

International Journal of Heat and Mass Transfer

journal homepage: www.elsevier.com/locate/ijhmt

Visualization study of steam condensation in triangular microchannels

Yongping Chen [a,*], Rui Wu [a], Mingheng Shi [a], Jiafeng Wu [a], G.P. Peterson [b]

[a] School of Energy and Environment, Southeast University, Nanjing, Jiangsu 210096, PR China
[b] Office of the President, Georgia Institute of Technology, Atlanta, GA 30332-0325, USA

ARTICLE INFO

Article history:
Received 20 November 2008
Received in revised form 9 April 2009
Accepted 13 April 2009
Available online 13 June 2009

Keywords:
Condensation
Microchannel
Flow pattern
Heat transfer

ABSTRACT

A visualization experiment is conducted to investigate the condensation of steam in a series of triangular silicon microchannels. The results indicate that droplet, annular, injection and slug-bubbly flow are the dominant flow patterns in these triangular silicon microchannels. With increased mass flow rate, or an increase in the hydraulic diameter under the same Reynolds number, the location at which the injection occurred is observed to move towards the channel outlet. The frequency of the injection increases, i.e. the flow of condensation instability is higher with increased inlet vapor Reynolds number, condensate Weber number and the prolongation of the injection location, or with a decrease in the hydraulic diameter of the channel. In addition, the wall temperature of the channel decreases along the condensation stream. The total pressure drop, the average condensation heat transfer coefficient and the average Nusselt number are observed to be larger with increased inlet vapor Reynolds number. Moreover, it is found that the condensation heat transfer is enhanced by a reduction in the channel scale.

© 2009 Elsevier Ltd. All rights reserved.

1. Introduction

Flow condensation in microchannels plays key role in micro heat pipes, chip laboratories, micro fuel cells and micro thermal systems [1]. With the addition of advanced micro electro mechanical system (MEMS) technology, it is relatively easy to fabricate microchannels whose diameters are less than 1 mm [2,3]. Recent experimental results indicate that the physical mechanisms of condensation in microchannels are quite different from that occurring in macro scale channels, since in most cases, surface tension and sheer stress between vapor and liquid layer are the dominate forces in the microchannels, as opposed to the more regular body forces, typically found in more common macro channels [1]. In addition, as recent microfluidic studies have demonstrated, the cross-sectional shape deeply influences the gas-liquid two-phase flow in microchannels [4].

Recognizing the significant potential of condensation heat transfer in microchannels, while somewhat limited, there are several studies on the flow condensation characteristics in microchannels. As early as the 1950s, Georgia [5] recognized that surface tension on a curved surface could induce a pressure gradient many times larger than that induced by gravity. Several theoretical or numerical investigations on condensation in microchannels have been presented [6–13]. Chen et al. developed a one-dimensional steady-state model of annular condensation in triangular [11] and rectangular [12] microchannels at constant heat flux conditions. The effect of surface tension is emphasized in the model along with the abnegation of the gravitational body force. However, the influence of the condensate distribution on the channel wall was neglected in the one dimensional model, which could lead to a distortion of the actual values and operational parameters. Recently, in order to give a more reliable theoretical description for micro condensation, Chen and coworkers [13] completed a three-dimensional simulation, which considered the condensate film distribution in rectangular microchannels with constant heat flux.

In addition to these original theoretical investigations, several experimental investigations involving condensation in mini/microchannels have been conducted. Garimella and coworker [14,15] presented an overview of the visualization study on condensation of refrigerants in minichannels. Experiments for condensation in round, square and rectangular tubes with hydraulic diameters in the range of 1–5 mm were reported and two phase flow regimes and patterns in minichannels were presented. An et al. [16,17] observed the flow patterns in round microchannels. Only plug flow, annular flow and bubbly flow were observed in round channel having the diameter of 0.468 mm, and it was found that the transition of the flow pattern will be deeply influenced by the mass flow rate. Médéric et al. [18] performed a visualization study of condensation flow patterns in tubes with diameters of 0.56, 1.1 and 10 mm. This observation provided sufficient evidence that the capillary force is the dominant force of flow condensation in channels whose diameters are less than 1 mm. Chen and Cheng [19] performed a visualization study of condensation in parallel silicon microchannels with hydraulic diameter of 75 μm, an intermittent flow of vapor

* Corresponding author. Tel.: +86 25 8379 3092; fax: +86 25 8361 5736.
E-mail address: ypchen@seu.edu.cn (Y. Chen).

0017-9310/$ - see front matter © 2009 Elsevier Ltd. All rights reserved.
doi:10.1016/j.ijheatmasstransfer.2009.04.034

Nomenclature

A_c, A	cross-sectional area and heat transfer area of a single channel, respectively
Bo	two-phase flow Bond number
Co	condensation number
c_p	specific heat of the cooling water
D	hydraulic diameter of channel
f_p	injection frequency
f	frequency of exposure
G	volume flow rate of the cooling water
g	acceleration due to gravity
h_1, h_2	enthalpy of the condensation flow at the inlet and outlet of the channel, respectively
L	channel length
M	injection period number
m_c	total mass flow rate
N	number of photograph
Nu	average Nusselt number of flow condensation
n	channel number
q	total heat flow rate
q'	heat flow rate removed from a single channel
Re_v	inlet vapor Reynolds number
T_{in}, T_{out}	inlet and outlet temperature of cooling water, respectively
t_b	average temperature after injection flow
t_f	average temperature before injection flow
$\bar{t}_f$	average temperature of condensation flow
t_{in}, t_{out}	inlet and outlet temperature of condensation flow, respectively
$t_w, \bar{t}_w$	wall temperature and average wall temperature of channel
We_l	condensate Weber number
$x_p, x_p/L$	location and dimensionless location of injection flow, respectively

Greeks

α	average heat transfer coefficient of flow condensation
γ	latent heat
Δp	total pressure drop of the condensation
μ_l, μ_v	dynamic viscosity of the condensate and the vapor, respectively
υ_v	kinematic viscosity of vapor
λ_f	thermal conductivity
ρ, ρ_l, ρ_v	density of cooling water, condensate and vapor, respectively
σ	surface tension coefficient

and condensate was observed. Subsequently, an experiment on condensation of steam in trapezoidal parallel microchannels having a hydraulic diameter of 82.8 μm was performed by Wu and Cheng [20]. Droplet flow, annular flow and injection flow were observed. Chen et al. [21] conducted a visualization investigation of condensation in triangular silicon microchannels with diameters less than 250 μm. The results indicated that the channel scale, heat flux, and mass flow rate all have significant influence on the condensation flow patterns, and droplet flow, annular flow and injection flow etc. were all observed. Of particular interest here was the new observation of injection flow at a constant frequency, which received increasing attention in the past several years. However, the measurement of heat transfer coefficient was not included in Chen's above work [19,21]. After that, Wu and coworkers [22] further studied the flow condensation in three sets of trapezoidal silicon microchannels, having hydraulic diameters of 53.0, 77.5 and 128.5 μm, respectively. Based on the experimental results, a correlation for the location of injection flow in function of the Reynolds number, condensation number and hydraulic diameter was proposed. More recently, Quan et al. [23] studied the injection flow of condensation in trapezoidal silicon microchannels at the basis of Wu et al. [20,22]. They found that the increase of steam mass flow rate, decrease of cooling rate or microchannel diameter tend to enhance the instability of the condensation film on the wall, resulting in the occurrence of injection flow further toward the outlet with an increase in occurrence frequency. Zhang et al. [24,25] also investigated the bubble emission and the multichannel effect of condensation in rectangular microchannels.

The measurement of the heat transfer coefficient is another important and difficult work in studying micro flow condensation. Garimella and Bandhauer [15] developed a technique for the measurement of condensation heat transfer coefficients in microchannels. And the measured heat transfer coefficient for the condensation of refrigerant R134a in a square microchannel with hydraulic diameter of 0.76 mm was found in the range of 2110–10,640 W m^{-2} K^{-1}. Cavallini et al. [26] measured the heat transfer coefficient for condensation of R134a and R410a inside multi-port minichannels having a hydraulic diameter of 1.4 mm. The heat transfer coefficient was found as high as 16,000 W m^{-2} K^{-1}, and it was proved that the condensation heat transfer will be enhanced with decreasing hydraulic diameter. An et al. [17] also measured the heat transfer coefficient in the round microchannels having the hydraulic diameters of 289–997 μm. They found the average Nusselt number increases with the increase of inlet vapor Reynolds number, and decreases with decreasing tube diameter, while the circumferential average heat transfer coefficient increases obviously with decreasing tube diameter.

As mentioned above, a few investigations of condensation in microchannels have been conducted in recent years. But the majority of the available experimental work are focused on millimeter or sub-millimeter scale channels, even though Wu et al. [20,22] have done efforts on the understanding of the micro condensation, but their studies are based on the trapezoidal channel. However, as the most commonly applied in micro heat pipe, flow condensation in triangular microchannels is still insufficient in current study. Despite Chen et al. [21] have contributed a flow map of condensation in triangular microchannels, heat transfer in triangular microchannels has not been measured in the past work. To address this issue and provide a more detailed experimental data, which to push the understanding of the condensation in triangular microchannels, a systemic experimental study on flow condensation in triangular silicon microchannels is performed in this paper. The flow patterns in triangular silicon microchannels with hydraulic diameters of 250 and 100 μm are recorded. In addition, the position and frequency of injection flow, wall temperature of channel, total pressure drop, average condensation heat transfer coefficient and average Nusselt number under different conditions are also measured in the paper.

2. Description of the experiment

2.1. Experimental setup

As shown in Fig. 1, parallel isosceles triangular microchannels with sidewalls inclined at 54.7°, whose hydraulic diameters D are 250 and 100 μm, are etched in the ⟨100⟩ silicon wafer by wet

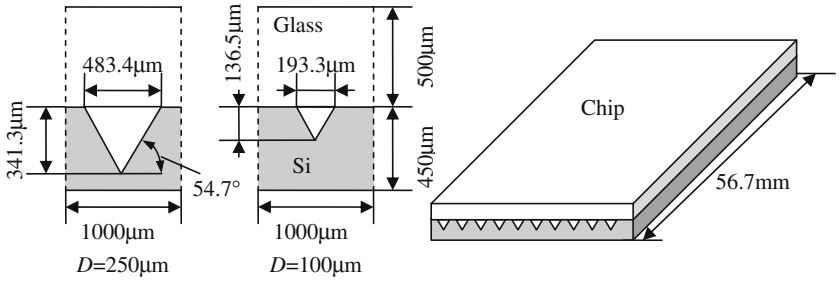

Fig. 1. Schematic of triangular silicon microchannel chip.

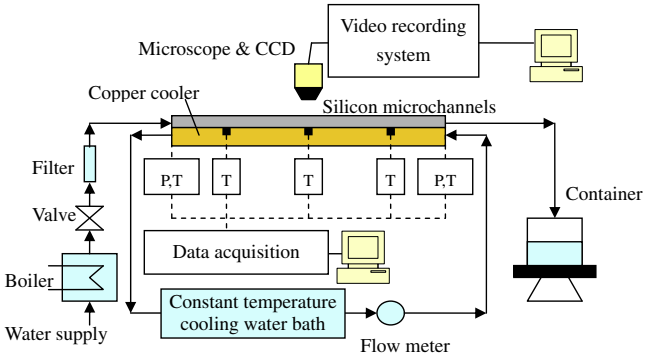

Fig. 2. Schematic of experimental setup.

TMAH solution and a Pyrex glass is anodic bonded on the top of the wafer. The number of channels in each silicon chip n is 10, and the length of each channel L is 56.7 mm.

Fig. 2 indicates the schematic of the experiment setup. Saturated steam, which is generated by the boiler, flows successively through the valve, filter and then arrives at the microchannel section in which the vapor condensates and releases heat to the cooling water in the copper cooler. Both the silicon chip and the copper cooler are fixed on an adiabatic workbench and compacted with each other. High-temperature thermally conductive grease is painted on the contact surfaces between the silicon chip and the cooper cooler in order to reduce the thermal contact resistance. The whole experimental section is covered by the thermal insulation materials to limit heat loss, except the place for photographing.

In the experiment, the temperature at the inlet and outlet of the condensation flow and cooling water, as well as the wall temperature of the silicon channel are measured by type T thermocouples (accuracy: ±0.1 °C). The pressure of inlet vapor is measured by high-temperature pressure sensor (accuracy: ±1.5 kPa). The volume flow rate of cooling water is measured by glass rotor flow meter (accuracy: ±0.4 L/h). Temperature and pressure data are collected by Agilent 34970A data acquisition. The condensation flow pattern is recorded by a microscope having a 2X objective lens and the maximum zoom ratio of 6.4, and a FASTCAM-NET-MAX3 high-speed video camera at the frequency of 125FPS or 250FPS. The injection location x_p is measured by vernier caliper (accuracy: ±0.02 mm). The different experimental conditions are applied by regulating the inlet saturated vapor pressure, and controlling the temperature and flow rate of the cooling water.

2.2. Data analysis

The frequency of the injection flow is calculated from the image number for one injection period recorded by the video recording system. For example, if the frequency of exposure is f and M injection periods are recorded by N photographs, the injection frequency f_p can be calculated as

$$f_p = \frac{fM}{N} \tag{1}$$

The total heat flow rate can be calculated as

$$q = c_p \rho G (T_{out} - T_{in}) \tag{2}$$

where T_{out}, T_{in}, G, c_p and ρ are outlet temperature, inlet temperature, volume flow rate, specific heat and density of the cooling water, respectively.

Since the ten channels etched in the wafer are parallel and identical, it is reasonable to assume that the same heat flow rate is released from each single triangular channel to the cooling water. Therefore, the heat flow rate removed from the sidewalls of a single triangular channel is

$$q' = \frac{q}{n} \tag{3}$$

The average heat transfer coefficient is

$$\alpha = \frac{q'}{A(\bar{t}_f - \bar{t}_w)} \tag{4}$$

where A is heat transfer area in a single channel, and $\bar{t}_w$ is the average wall temperature of channel, which is the algebraic average of the measured temperatures on the wall surface. $\bar{t}_f$ is the average temperature of condensation flow, which is computed by

$$\bar{t}_f = \frac{t_f x_p + t_b (L - x_p)}{L} = \frac{t_{in} + t_{out}}{2} + \frac{x_p}{L} \frac{t_{in} - t_{out}}{2} \tag{5}$$

where t_f is the average temperature of the vapor before the injection flow, which can be regarded as the inlet saturated steam temperature, t_{in}, t_b is the average temperature after injection, which is approximately equal to the average of the saturated steam temperature t_{in} and the outlet condensation flow temperature t_{out}.

The total condensation mass flow rate can be calculated as

$$m_c = \frac{q}{h_1 - h_2} \tag{6}$$

where h_1 and h_2 are the enthalpy of the condensation flow at the inlet and outlet of the channel.

The inlet vapor Reynolds number Re_v and the condensate Weber number We_l are derived by

$$Re_v = \frac{m_c D}{n \upsilon_v \rho_v A_c} \tag{7}$$

$$We_l = \frac{\rho_l D}{\sigma} \left(\frac{m_c}{n \rho_l A_c} \right)^2 \tag{8}$$

where A_c is the cross-sectional area of channel, ρ_v and ρ_l are the density of the saturated vapor and condensate, respectively, σ and υ_v are the surface tension coefficient and saturated vapor viscosity, respectively.

The Bond number, Bo, condensation number, Co, and average Nusselt number of flow condensation, Nu, in triangular microchannel are

$$Bo = \frac{g(\rho_l - \rho_v)D^2}{\sigma} \quad (9)$$

$$Co = \frac{h_1 - h_2}{\gamma} \quad (10)$$

$$Nu = \frac{\alpha D}{\lambda_f} \quad (11)$$

where g, γ and λ_f are acceleration due to gravity, latent heat and thermal conductivity, respectively.

Based on the data error analysis, the uncertainties of various parameters in this paper are listed in Table 1.

3. Experimental results and discussion

3.1. Flow patterns

Differing from the larger or macro condensation, which is dominated by gravity and buoyancy, the condensation flow pattern in microchannels is dominated by surface tension and shear stress on vapor-liquid interface. As shown in Fig. 3, the flow patterns are droplet flow, annular flow, injection flow and slug-bubbly flow along the triangular microchannel. Compared with the experimental results reported by Wu and Cheng [20] and An et al. [16], the condensation flow patterns occurring in the triangular silicon microchannels is similar to the flow patterns in trapezoidal microchannels, but different from the flow patterns in circular microchannels.

Since the silicon surface is a hydrophobic surface, droplet condensation takes place near the inlet of the triangular microchannels (see Fig. 3(b)). As the accumulation of the condensate, the channel side wall will entirely be covered by the condensate, and the flow pattern will be converted to annular flow (see Fig. 3(c)) at the downstream of the droplet flow.

Table 1
Uncertainties of parameters.

Parameters	Uncertainties (%)	Parameters	Uncertainties (%)
x_p/L	1.41	Re_v	8.02
f_p	3.15	We_l	11.3
q	7.98	Bo	1.01
m_c	7.99	Co	0.32
α	8.09	Nu	8.10

At the end of the annular flow pattern, a periodic injection flow pattern is observed (see Fig. 3(d)). Injection flow is the alternation between annular flow and slug-bubbly flow. Fig. 4 lists two periods of injection flow, including the injection growth and break. As shown in Fig. 4, two bubbles are emitted within about 0.232 s in D = 250 μm triangular microchannel having the inlet vapor Reynolds number, Re_v, of 392.1 and the heat flow rate, q, of 42.52 W. And it is found the frequency of injection is quite steady. Although the injection flow pattern is also found in condensation in trapezoidal microchannels, the injection period in triangular channel measured in this paper is a little longer than that measured in trapezoidal microchannels by Quan et al. [23].

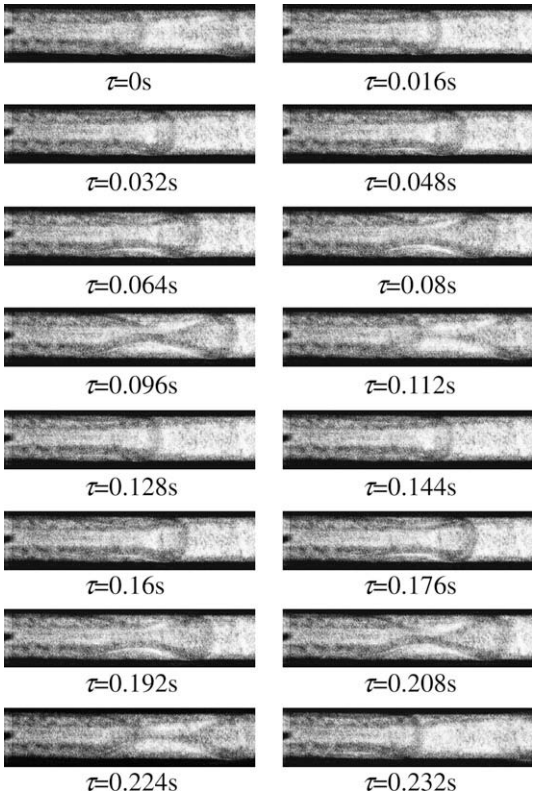

Fig. 4. Injection flow in triangular microchannel (D = 250 μm, Bo = 0.01067, q = 42.52 W, Re_v = 392.1, We_l = 0.002135, x_p/L = 0.5291, f = 125FPS, f_p = 8.417 Hz).

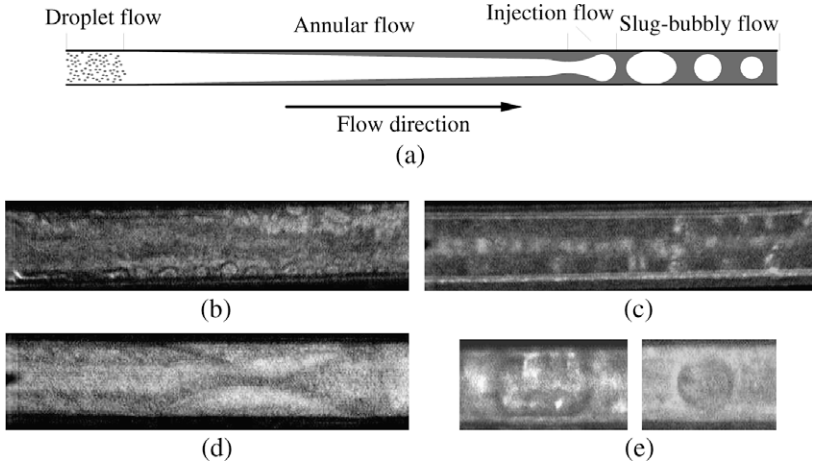

Fig. 3. Flow patterns in triangular microchannel: (a) Schematic diagram; (b) Droplet flow; (c) Annular flow; (d) Injection flow and (e) Slug-bubbly flow.

After the injection flow, the vapor in emitted bubbles will be further cooled in the slug-bubbly flow region (see Fig. 3(e)). Finally, the bubbles are gradually condensed, shrank and submerged in the condensate.

In addition, the mechanisms of flow condensation in microchannels should also be different from the adiabatic liquid–gas two-phase flow [27–33]. The comparison between the condensation flow and adiabatic liquid–gas two-phase flow in microchannels is conducted. Fig. 5 illustrates the adiabatic liquid–gas two-phase flow patterns in the triangular microchannel by Zhao and Bi [33]. As shown in the figure, capillary bubble flow, slug flow, churn flow and annular flow were observed, respectively, under different experimental conditions. More specifically, under a certain operating condition, the flow pattern is not altered along the adiabatic two-phase flow. However, different flow patterns exist simultaneously along the condensation stream. The injection flow, which can be regarded as the characteristic flow pattern for condensation in microchannels, has not been observed in the adiabatic liquid-gas two-phase flow.

3.2. Effects of experimental condition to injection flow

Although injection flow is an unstable flow pattern, the location and the frequency of the injection flow is not altered under a certain operating condition.

Fig. 6 shows the variation of dimensionless injection location, x_p/L, versus the inlet vapor Reynolds number, Re_v. The injection flow occurring in the channel and the similar condensation numbers Co in different microchannel chips are ensured by the cooling water with different inlet temperature T_{in} but the same volume flow rate G. As shown in Fig. 6, x_p/L increases with the increase of Re_v, which indicates the injection flow location moves towards the outlet when the mass flow rate increases. It is also indicated by the figure that the location of injection flow is also influenced by the hydraulic diameter, and x_p/L increases with the increase of hydraulic diameter D at the same Re_v.

The surface tension is another important factor for the location of injection flow. As shown in Fig. 7, x_p/L also increases with the increase of We_l, which indicates the ratio of inertia force and surface tension in the condensate. Based on the experimental data, the correlation of x_p/L, Re_v, We_l and D/L is presented as

$$x_p/L = 5.939 \times 10^3 \mathrm{Re}_v^{0.695} We_l^{0.302} (D/L)^{2.149} \quad (12)$$

The locations of injection flow predicted by Eq. (12) are compared with the experimental data in Fig. 8 and Table 2. The correlation coefficient and the maximum deviation of Eq. (12) from the experimental data are 0.9851 and 11.8%, respectively.

Figs. 9 and 10 present the injection frequency f_p versus Re_v and We_l. The frequency f_p will increase with the increase of Re_v or We_l in the same channel. Fig. 11 illustrates the relationship between the injection frequency f_p and the dimensionless injection location x_p/L. The frequency is lower when the injection occurs in the upper stream of the channel. At the same time, the hydraulic diameter D has a significantly effect on the flow condensation instability in the microchannels. The vapor–liquid interface is more unstable in the smaller channel, in which f_p is much higher. Based on the experimental data, the correlation of f_p, Re_v, We_l and D/L in triangular microchannels is presented as

$$f_p = 0.188 \mathrm{Re}_v^{0.992} We_l^{0.436} (D/L)^{-0.132} \quad (13)$$

The correlation coefficient and the maximum deviation of Eq. (13) from the experimental data are 0.9540 and 25.9%, respectively. Fig. 12 and Table 2 show the comparison between the predicted injection frequency values from Eq. (13) and the experimental data.

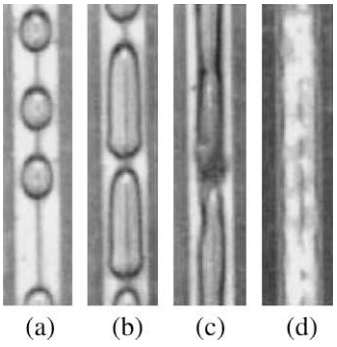

Fig. 5. Adiabatic two-phase flow patterns in triangular microchannel of D = 866 μm [33]: (a) Capillary bubble flow (u_{gas} = 0.2 m/s, u_{water} = 0.1 m/s); (b) Slug flow (u_{gas} = 0.4 m/s, u_{water} = 0.1 m/s); (c) Churn flow (u_{gas} = 5.5 m/s, u_{water} = 0.1 m/s) and (d) Annular flow (u_{gas} = 85 m/s, u_{water} = 0.1 m/s).

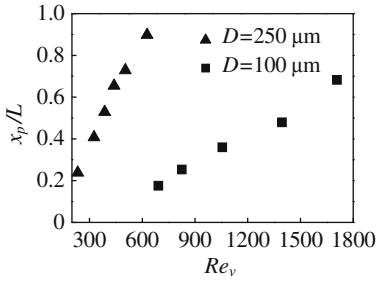

Fig. 6. Dimensionless injection location versus the inlet vapor Reynolds number (D = 250 μm: Bo = 0.01073, Co = 1.07, T_{in} = 58.6 °C, G = 10.0 L/h, f = 125FPS; D = 100 μm: Bo = 0.001719, Co = 1.09, T_{in} = 42.1 °C, G = 10.0 L/h, f = 125FPS or 250FPS).

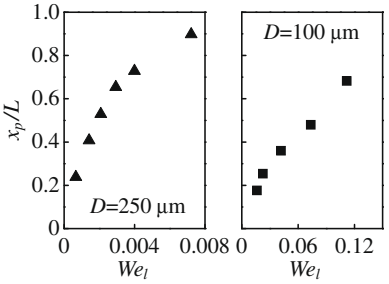

Fig. 7. Dimensionless injection location versus condensate Weber number. (The same condition with Fig. 6.)

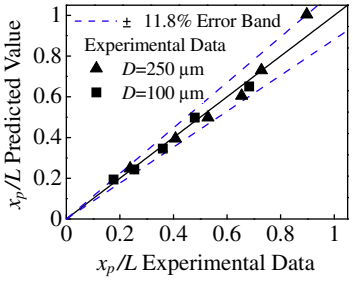

Fig. 8. Comparison between the predicted and experimental values of dimensionless injection location. (The same condition with Fig. 6.)

Table 2
Experimental data points and fitting values. (The same condition with Fig. 6.)

Re_v	We_l	x_p/L			f_p (Hz)			Nu		
		Experimental data	Fitting value	Relative error (%)	Experimental data	Fitting value	Relative error (%)	Experimental data	Fitting value	Relative error (%)
D = 250 μm triangular microchannel										
627.9	7.215×10^{-3}	0.8977	1.004	11.8	33.88	26.90	−20.6	1.727	1.961	13.6
499.7	3.993×10^{-3}	0.7284	0.7304	0.275	16.69	16.73	0.252	1.624	1.642	1.10
440.1	2.935×10^{-3}	0.6543	0.6052	−7.50	11.13	12.78	14.9	1.722	1.751	1.71
392.1	2.135×10^{-3}	0.5291	0.5097	−3.67	8.417	9.849	17.0	1.679	1.551	−7.62
326.0	1.423×10^{-3}	0.4074	0.3948	−3.09	5.741	6.928	20.7	1.374	1.419	3.22
232.8	6.624×10^{-3}	0.2381	0.2482	4.24	4.280	3.563	−16.8	1.334	1.210	−9.30
D = 100 μm triangular microchannel										
1708	0.1119	0.6825	0.6506	−4.68	–*	–	–	2.142	1.972	−7.94
1395	7.354×10^{-2}	0.4797	0.4981	3.82	146.8	183.7	25.1	2.043	1.799	−12.0
1055	4.174×10^{-2}	0.3598	0.3458	−3.90	86.47	108.9	25.9	1.491	1.588	6.51
824.8	1.624×10^{-2}	0.2540	0.2429	−4.35	65.92	65.64	−0.425	1.270	1.407	10.8
691.4	2.284×10^{-2}	0.1764	0.1939	9.92	57.54	47.52	−17.4	1.246	1.302	4.53

* Too high frequency to be recorded.

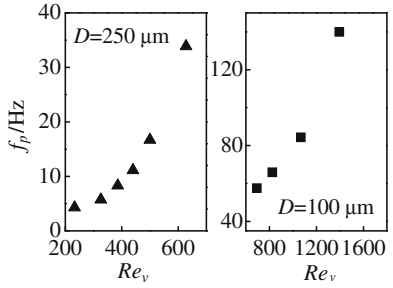

Fig. 9. Injection frequency versus the inlet vapor Reynolds number. (The same condition with Fig. 6.)

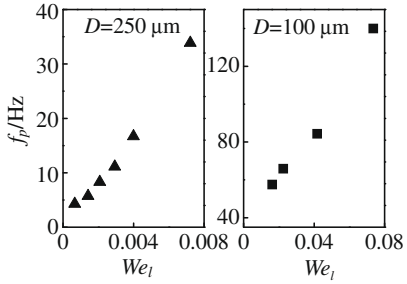

Fig. 10. Injection frequency versus the condensate Weber number. (The same condition with Fig. 6.)

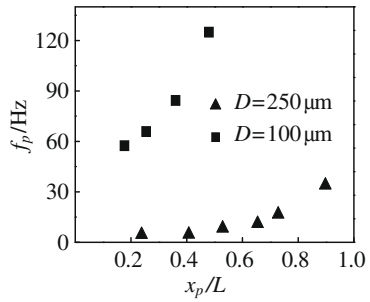

Fig. 11. Injection frequency versus the injection location. (The same condition with Fig. 6.)

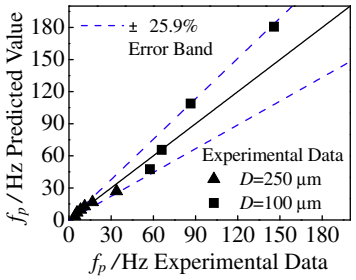

Fig. 12. Comparison between the predicted and experimental values of injection frequency. (The same condition with Fig. 6.)

3.3. Characteristics of condensation flow and heat transfer

Fig. 13 shows the wall temperature distribution of condensation in triangular microchannel with a diameter of 250 μm. It is found that the wall temperature decreases along the flow direction, and the average wall temperature will increase with the increase of inlet vapor Reynolds number, Re_v.

Fig. 14 presents the total pressure drop of the condensation Δp versus the inlet vapor Reynolds number Re_v. As illustrated in the figure, Δp increases with the increase of Re_v nearly linearly, which is similar to the experimental results conducted by An et al. [16] in the circular microchannels.

Figs. 15 and 16 are the plots of the average condensation heat transfer coefficient α and the average Nusselt number Nu versus the inlet vapor Reynolds number Re_v, respectively. As shown in

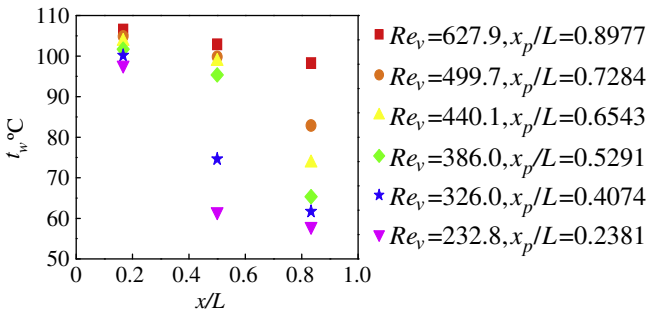

Fig. 13. Wall temperature distribution (D = 250 μm, the same condition with Fig. 6).

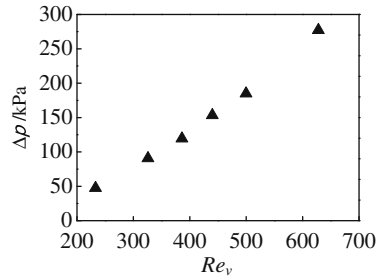

Fig. 14. The total pressure drop of the condensation versus the inlet vapor Reynolds number. (D = 250 μm, the same condition with Fig. 6.)

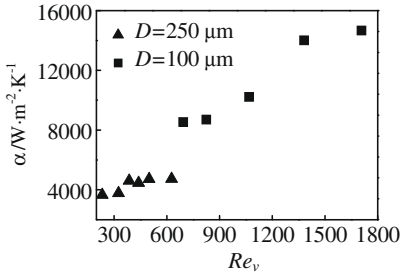

Fig. 15. Average condensation heat transfer coefficient versus inlet vapor Reynolds number. (The same condition with Fig. 6.)

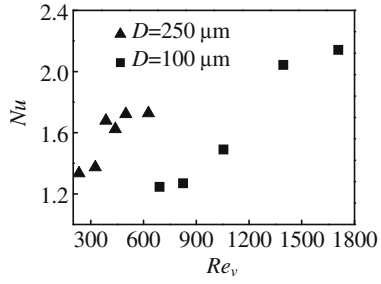

Fig. 16. Average Nusselt number versus inlet vapor Reynolds number. (The same condition with Fig. 6.)

the figures, for the larger Re_v, the injection location is postponed, and the droplet and annular flow regime are extended, while the slug-bubbly flow regime, whose heat transfer coefficient is much less than that in the droplet and annular flow regime, is truncated. Therefore, α and Nu are larger at larger Re_v in the same channel. And the condensation heat transfer coefficient in 100 μm microchannel is much higher than what in 250 μm microchannel, which indicates that the flow condensation heat transfer is enhanced significantly by the reduction of the channel diameter. However, it must be addressed, in despite of the increase of condensation heat transfer coefficient, Nu decreases with the decrease of channel hydraulic diameter. Based on the experimental data, the correlation of Nu, Re_v and D/L in triangular silicon microchannels can be expressed as

$$Nu = 1.329\mathrm{Re}_v^{0.480}(D/L)^{0.500} \quad (14)$$

The correlation coefficient and the maximum deviation of Eq. (14) from the experimental data are 0.8731 and 13.6%, respectively. Fig. 17 and Table 2 show the comparison of Nu between the predicted results and the experimental data.

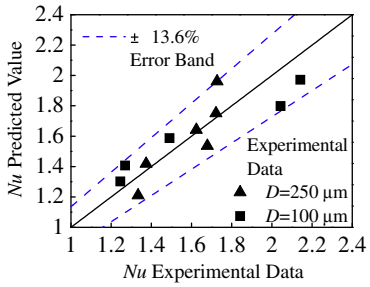

Fig. 17. Comparison between the predicted and experimental values of Nusselt number. (The same condition with Fig. 6.)

4. Conclusions

A visualization experiment is conducted to investigate the flow condensation in the silicon triangular microchannels with hydraulic diameters of 250 and 100 μm. The flow patterns and the heat transfer characteristics are all acquired. Based on the experimental data, the formulas of injection location, injection frequency and condensation Nusselt number in triangular silicon microchannels are presented. The conclusions can be summarized as

(1) Dominated by the surface tension and shear stress on vapor-liquid interface, rather than the traditional body force such as gravity and buoyancy in the normal scale channels, the droplet flow, annular flow, injection flow and slug-bubbly flow are observed in flow condensation along the flow direction in triangular microchannel.
(2) Injection flow is a transition flow pattern from the annular flow to the slug-bubbly flow. Although the injection flow is an unstable flow pattern, the location and the frequency of injection keep stable under a certain condition.
(3) The injection flow will be postponed with the increase of mass flow rate in the same microchannel. In addition, at the same inlet vapor Reynolds number, injection location is observed to move towards the channel outlet with increasing hydraulic diameter of the channel. The injection frequency increases with the increase of inlet vapor Reynolds number and condensate Weber number, as well as the prolongation of injection location. The injection frequency in smaller channels is much lager than that in the larger channel, i.e. the vapor–liquid interface is more unstable in a smaller channel.
(4) The wall temperature of the channel decreases along the condensation stream. And the total pressure drop of the condensation increases with the increase of inlet vapor Reynolds number.
(5) Both the average condensation heat transfer coefficient and the average condensation Nusselt number increase with the increase of inlet vapor Reynolds number. The reduction of diameter has a significant role in the enhancement of condensation heat transfer. However, under the same inlet vapor Reynolds number, the average condensation Nusselt number will be reduced as the diameter decreases.

Acknowledgements

The authors gratefully acknowledge the support provided by National Natural Science Foundation of China (No. 50806012).

References

[1] Y.P. Chen, M.H. Shi, P. Cheng, G.P. Peterson, Condensation in microchannels, Nanoscale Microscale Thermophys. Eng. 12 (2008) 117–143.

[2] E. Cormac, D. Tara, D. Mark, O. Cian, S. Oral, Direct comparison between five different microchannels, part 1: channel manufacture and measurement, Heat Transfer Eng. 26 (2005) 79–88.
[3] C. Perret, J. Boussey, C. Schaeffer, M. Coyaud, Analytic modeling, optimization, and realization of cooling devices in silicon technology, IEEE Trans. Compon. Packag. Technol. 23 (2000) 665–672.
[4] N. Ichikawa, K. Hosokawa, R. Maeda, Interface motion of capillary-driven flow in rectangular microchannel, J. Colloid Interface Sci. 280 (2004) 155–164.
[5] R. Georgia, Film condensation on finely rippled surfaces with consideration of surface tension, Z. Angew. Math. Phys. 5 (1954) 36–49.
[6] T.S. Zhao, Q. Liao, Theoretical analysis of film condensation heat transfer inside vertical mini triangular channels, Int. J. Heat Mass Transfer 45 (2002) 2829–2842.
[7] X.Z. Du, T.S. Zhao, Analysis of film condensation heat transfer inside a vertical micro tube with consideration of the meniscus draining effect, Int. J. Heat Mass Transfer 46 (2003) 4669–4679.
[8] H.S. Wang, J.W. Rose, H. Honda, A theoretical model of film condensation in square section horizontal microchannels, Chem. Eng. Res. Des. 82 (2004) 430–434.
[9] H.S. Wang, J.W. Rose, A theory of film condensation in horizontal noncircular section microchannels, ASME J. Heat Transfer 127 (2005) 1096–1105.
[10] H.S. Wang, J.W. Rose, Film condensation in horizontal microchannels: effect of channel shape, in: Proceedings of the 3rd International Conference on Microchannels and Minichannels, Toronto, Ont., Canada, 2005, pp. 729–35.
[11] Y.P. Chen, J.F. Wu, M.H. Shi, G.P. Peterson, Numerical simulation for steady annular condensation flow in triangular microchannels, Int. Comm. Heat Mass Transfer 35 (2008) 805–809.
[12] J.F. Wu, Y.P. Chen, M.H. Shi, C.M. Xiao, C.B. Zhang, Simulation for annular condensation flow in rectangular microchannels, J. Eng. Thermophys. 29 (2008) 1924–1926.
[13] J.F. Wu, Y.P. Chen, M.H. Shi, P.P. Fu, G.P. Peterson, Three dimensional numerical simulation for annular condensation in rectangular microchannels, Nanoscale Microscale Thermophys. Eng. 13 (2009) 13–29.
[14] S. Garimella, Condensation flow mechanisms in microchannels: basis for pressure drop and heat transfer models, in: Proceedings of the 1st International Conference on Microchannels and Minichannels, Rochester, New York, 2003, pp. 181–92.
[15] S. Garimella, T.M. Bandhauer, Measurement of condensation heat transfer coefficients in microchannel tubes, ASME, Heat Transfer Division, Fluid-Physics and Heat Transfer for Macro- and Micro-scale Gas–Liquid and Phase-Change Flows, New York, 2001, pp. 243–49.
[16] G. An, J.M. Li, B.X. Wang, Experimental study on condensation heat transfer in microtube, J. Eng. Thermophys. 24 (2003) 79–81.
[17] G. An, J.M. Li, H.Y. Zhang, B.X. Wang, Investigation on film condensation heat transfer characteristics in horizontal micro/mini tubes, J. Eng. Thermophys. 27 (2006) 652–654.
[18] B. Médéric, M. Miscevic, V. Platel, P. Lavieille, J.L. Joly, Experimental study of flow characteristics during condensation in narrow channels: the influence of the diameter channel on structure patterns, Superlattices Microstruct. 35 (2004) 573–586.
[19] Y.P. Chen, P. Cheng, Condensation of steam in silicon microchannels, Int. Comm. Heat Mass Transfer 32 (2005) 175–183.
[20] H.Y. Wu, P. Cheng, Condensation flow patterns in silicon microchannels, Int. J. Heat Mass Transfer 48 (2005) 2186–2197.
[21] Y.P. Chen, J. Li, G.P. Peterson, Influence of hydraulic diameter on flow condensation in silicon microchannels, in: Proceedings of 13th International Heat Transfer Conference, Sydney, Australia, 2006.
[22] H.Y. Wu, M.M. Yu, P. Cheng, X.Y. Wu, Injection flow during steam condensation in silicon microchannels, J. Micromech. Microeng. 17 (2007) 1618–1627.
[23] X.J. Quan, P. Cheng, H.Y. Wu, Transition from annular flow to plug/slug flow in condensation of steam in microchannels, Int. J. Heat Mass Transfer 51 (2008) 707–716.
[24] W. Zhang, J.L. Xu, Flow pattern and multichannel effect of steam condensation in silicon microchannels, J. Eng. Thermophys. 29 (2008) 605–608.
[25] W. Zhang, J.L. Xu, J.R. Thome, Periodic bubble emission and appearance of an ordered bubble sequence (train) during condensation in a single microchannel, Int. J. Heat Mass Transfer 51 (2008) 3420–3433.
[26] A. Cavallini, D. Del Col, L. Doretti, M. Matkovic, L. Rosetto, C. Zilio, Condensation heat transfer inside multi-port minichannels, in: Proceedings of 2nd International Conference on Microchannels and Minichannels, Rochester, New York, 2004, pp. 625–32.
[27] K.A. Triplett, S.M. Ghiaasiaan, S.I. Abdel-Khalik, D.L. Sadowski, Gas–liquid two-phase flow in microchannels, part I: two-phase flow patterns, Int. J. Multiphase Flow 25 (1999) 377–394.
[28] W.L. Chen, M.C. Twu, C. Pan, Gas–liquid two-phase flow in micro-channels, Int. J. Multiphase Flow 28 (2002) 1235–1247.
[29] A. Serizawa, Z. Feng, Z. Kawara, Two-phase flow in microchannels, Exp. Therm. Fluid Sci. 26 (2002) 703–714.
[30] P.M.Y. Chung, M. Kawaji, A. Kawahara, Y. Shibata, Two-phase flow through square and circular microchannels-effects of channel geometry, J. Fluids Eng. 126 (2004) 546–552.
[31] M. Dang, I. Hassan, R. Muwanga, Adiabatic two phase flow distribution and visualization in scaled microchannel heat sinks, Exp. Fluids 43 (2007) 873–885.
[32] T.S. Zhao, Q.C. Bi, Pressure drop characteristics of gas–liquid two-phase flow in vertical miniature triangular channels, Int. J. Heat Mass Transfer 44 (2001) 2523–2534.
[33] T.S. Zhao, Q.C. Bi, Co-current air–water two-phase flow patterns in vertical triangular microchannels, Int. J. Multiphase Flow 27 (2001) 765–782.